International Journal for Housing Science and Its Applications
Publish August 10, 2025. Volume 46, Issue 4 Pages 4670-4679

https://doi.org/10.70517/ijhsa464310

The Mechanism of Groundwater Seepage on the Stability of Geotechnical Foundation Engineering

Peng Li[1,*]
[1] School of Civil and Transportation Engineering of Henan University of Urban Construction Pingdingshan, Henan, 467002, China
Corresponding authors: (e-mail: lipeng@huuc.edu.cn).

Abstract Groundwater seepage is a key factor affecting foundation stability in geotechnical engineering, and its complex multi-field coupling characteristics put forward higher requirements for numerical simulation and parameter inversion. Aiming at the limitations of traditional methods in modeling and parameter identification of non-homogeneous seepage field, this paper proposes an inversion algorithm based on PINNs, which is combined with the finite element method to construct a framework for solving the positive groundwater seepage problem. The influence of seepage on the displacement, surface settlement and overall stability of the ground connecting wall is systematically analyzed through the case study of the foundation pit of a cross-river highway bridge in Southwest China. The results show that the PINNs algorithm can efficiently invert the seepage parameters, and the relative errors in solving the hydraulic conductivity coefficients T_1-T_3 are less than 0.009%, and the relative errors in the water storage coefficients S_1-S_3 are controlled within 0.05%. The horizontal displacement of the ground connecting wall under seepage is up to 52.02mm, the surface settlement is in the order of 3.16-18.39mm, and the safety coefficient is reduced to 5.52-5.78 due to fluid-solid coupling. This study provides a new numerical method and engineering reference for the assessment of the stability of geotechnical engineering under complex geological conditions.

Index Terms geotechnical engineering, groundwater seepage, parametric inversion, PINNs, finite element method

I. Introduction

Groundwater is a very important natural resource on earth, which is one of the hydrogeological elements constituting the development conditions of geotechnical engineering. In geotechnical engineering, groundwater has an important role, not only can solidify the soil, but also can play the role of cooling the soil, but it also has its harmfulness, if it is not prevented and controlled, it will bring negative impacts on geotechnical engineering [1], [2]. If the groundwater rises and falls regularly, it will cause very serious harm to the geotechnical engineering. The change of groundwater rise and fall can directly induce uneven and unbalanced shrinkage and expansion deformation of expansive geotechnical soil, and it will cause the frequency of shrinkage and expansion of geotechnical soil to increase, which will lead to cracks, landslides, mudslides and a series of serious damages and destructions of buildings, especially light buildings [3]-[6]. Groundwater in its natural state, its dynamic water pressure is relatively weak, under normal conditions will not pose a serious threat, if man-made factors lead to the natural dynamics of groundwater out of balance, under the action of the dynamic water pressure in the loose, often lead to serious geotechnical engineering hazards, for example, the pit surge, pipe surge and quicksand, which directly affects the entire construction project as well as the quality of the project [7]-[10].

Groundwater seepage problem is one of the important research contents in geotechnical engineering, and groundwater seepage refers to the flow process of groundwater from high-pressure area to low-pressure area in geotechnical body [11]. Groundwater has a certain ability to move, and its seepage characteristics are mainly affected by permeability, saturation, pore structure of infiltration media and permeability of infiltration media [12], [13]. In geotechnical engineering, groundwater seepage has an important impact on the mechanical properties of soil and rock, structural safety, and environmental protection [14], [15]. Therefore, understanding the mechanism and law of groundwater seepage on the stability of the project and taking reasonable and effective control and management measures are of great significance for the design and construction of geotechnical engineering.

In this paper, we first establish a solution model for the positive groundwater seepage problem based on the finite element method, and clarify the unsteady flow solution conditions and discrete format. The PINNs-driven seepage parameter inversion framework is proposed to realize the joint identification of homogeneous and inhomogeneous medium parameters. Groundwater seepage in the process of foundation pit excavation is introduced, and the effects of groundwater seepage on the stability of foundation pit engineering are summarized. The two-dimensional

unsteady flow in a nonhomogeneous isotropic pressurized aquifer is selected as an ideal model for calculation to verify the effectiveness of PINNs algorithm. Through the case of a large-scale foundation pit project in Southwest China, we quantitatively analyze the deformation of ground-connected wall, surface settlement and the change rule of structural safety coefficient under the action of seepage flow.

II. Groundwater seepage model solution and parameter inversion based on PINNs algorithm

Groundwater seepage in geotechnical engineering is characterized by multi-physical field coupling, significant spatial and temporal variability of parameters, and its dynamic effect directly affects the stability and durability of foundation structures. The traditional numerical simulation method relies on a priori parameter settings and is susceptible to model simplification errors in the inversion of seepage field in non-homogeneous media; while the parameter inversion method based on gradient optimization is sensitive to the amount of observed data and the initial guessing value, making it difficult to deal with high-dimensional nonlinear problems. In recent years, physical information neural networks (PINNs) provide a new idea for seepage parameter inversion due to their advantages of integrating data-driven and physical constraints.

II. A.Numerical Methods for Positive Groundwater Seepage Problems

Regardless of which parametric inversion method is used, it is necessary to solve the positive problem for the groundwater flow problem. For the two-dimensional unsteady flow fixed solution problem, the governing equations are as follows:

$$\frac{\partial}{\partial x}\left(T\frac{\partial H}{\partial x}\right)+\frac{\partial}{\partial y}\left(T\frac{\partial H}{\partial y}\right)-Q\delta(x-x_0,y-y_0) = S\frac{\partial H}{\partial t},(x,y)\in\Omega,t>0 \tag{1}$$

$$H\big|_{t=0}=H_0(x,y),(x,y)\in\Omega \tag{2}$$

$$H\big|_{\Gamma_1}=H_1,(x,y)\in\Gamma_1 \tag{3}$$

$$\left.\frac{\partial H}{\partial n}\right|_{\Gamma_2}=q(x,y,t),(x,y)\in\Gamma_2 \tag{4}$$

where H is the head (m); Q is the pumping volume $\left(m^3\cdot d^{-1}\right)$; δ is the Dirac function; (x_0,y_0) are the coordinates of the pumping wells; T is the hydraulic conductivity coefficient $\left(m^2\cdot d^{-1}\right)$; S is the storage coefficient, which is dimensionless; Γ_1, Γ_2 are the boundaries of Ω, and $H_0(x,y)$, $H_1(x,y)$, and $q(x,y,t)$ are the initial and boundary conditions, respectively.

The above problems can be solved numerically by finite element or finite difference, and in this paper, we use the finite element numerical computation method to solve the problem of unsteady flow fixed solution model.

Assuming that H_h is a set of triangular dissections of the outer surface of Ω, which satisfies

$$\max_{\tau\in H_h} diam(\tau)\le h \tag{5}$$

where $diam(\tau)$ is the maximum length of the region dissected into triangular diameters, and E_h is taken to be a finite-dimensional subspace.

Introduce the inner product on the subspace E_h:

$$(f,g)=\iint_{\Omega} fg\,dxdy \tag{6}$$

Take any $v(x,y,t)\in E_h$ and satisfy $v\,|_{\Gamma}=0$, multiply $v(x,y,t)\in E_h$ by the two ends of equation (1), and integrate over Ω to obtain:

$$T(\nabla^2 H,v)-(Q\delta(x-x_0,y-y_0),v)=S(\partial_t H,v) \tag{7}$$

The above equation is obtained using Green's formula:

$$\begin{aligned}&-T\iint_{\Omega}\nabla H(x,y,t)\nabla v dxdy-\iint_{\Omega}Q\delta(x-x_0,y-y_0)vdxdy+T\int_{\Gamma}n\cdot\nabla Hdxdy\\&=S\iint_{\Omega}\partial_t H(x,y,t)vdxdy\end{aligned}\tag{8}$$

can be obtained using the boundary conditions:

$$\begin{aligned}&-T\iint_{\Omega}\nabla H(x,y,t)\nabla v dxdy-\iint_{\Omega}Q\delta(x-x_0,y-y_0)vdxdy\\&=S\iint_{\Omega}\partial_t H(x,y,t)vdxdy\end{aligned}\tag{9}$$

This follows from the properties of the Dirac (Dirac) generalized function:

$$\begin{aligned}&S\iint_{\Omega}\partial_t H(x,y,t)vdxdy+H\iint_{\Omega}\nabla H(x,y,t)\nabla v dxdy\\&+Qv(x_0,y_0)=0\end{aligned}\tag{10}$$

Take the approximate solution of the equation in the following form:

$$H(x,y,t)\approx\sum_{j=1}^{N}H_j(t)\phi_j(x,y)\tag{11}$$

where $\{\phi_j(x,y)\}_{j=1}^{N}$ is the basis function of the standard finite element, substituting into equation (9) yields

$$\begin{aligned}&S\sum_{i=1}^{N}H_i'(t)(\phi_i,\phi_j)+T\sum_{i=1}^{N}H_i(t)(\nabla\phi_i,\nabla\phi_j)\\&+Q\phi_j(x_0,y_0)=0\quad j=1,2,\cdots,N\end{aligned}\tag{12}$$

If the order:

$$H=(H_1(t),H_2(t),\cdots,H_N(t))^T\tag{13}$$

$$H'=\left(\frac{dH_1(t)}{dt},\frac{dH_2(t)}{dt},\cdots,\frac{dH_N(t)}{dt}\right)^T\tag{14}$$

With the help of the initial condition (2), the following finite element discretization in matrix form can be obtained:

$$\begin{cases}SAH'+TBH=F_1\\H\big|_{t=0}=H_0(x_i,y_i)\end{cases}\tag{15}$$

Among them:

$$A_{ij}=\left(\phi_i,\phi_j\right)=\iint_{\Omega}\Omega\phi_i\phi_j dxdy\tag{16}$$

$$B_{ij}=\left(\nabla\phi_i,\nabla\phi_j\right)=\iint_{\Omega}\nabla\phi_i\nabla\phi_j dxdy\tag{17}$$

$$F_{1_j}=-Q\phi_j(x_0,y_0)\tag{18}$$

A differential approximation is used for the time derivative of equation (15), assuming the value of H_t at moment t:

$$\frac{dH}{dt}=\frac{H_{t+\Delta t}-H_t}{\Delta t} \tag{19}$$

Substituting into (15) gives:

$$\left(S\frac{A}{\Delta t}+TB\right)H_{t+\Delta t}=S\frac{A}{\Delta t}H_t+F_1 \tag{20}$$

This leads to a numerical solution for H at any point in the region and at any moment in time.

II. B.Identification of seepage parameters based on PINNS algorithm

The PINNs algorithm not only enables Darcy flow simulation, but also inverts the seepage parameters based on measured or simulated data of the head, which is shown in Fig. 1.

In the inversion of homogeneous seepage parameters, the loss term MSE_{Data}, which measures the deviation between the measured data and the predicted values, and its weight ω_D, are added based on the loss function of the forward head solution and the H-value $H(x_D)$ of the measured point x_D:

$$\omega_D MSE_{Data}=\omega_D\frac{1}{|\tau_D|}\sum_{x\in\tau_D}\left\|\hat{H}(x;\theta)-H(x_D)\right\|_2^2 \tag{21}$$

Where: τ_D is the set composed of measured data. Similarly, the final neural network parameter $\hat{\theta}$ and homogeneous seepage parameter $\hat{K}$ can be obtained by the optimization algorithm for the total loss function.

When the PINNs algorithm performs the inversion of non-homogeneous seepage parameters, since K varies with x, it is necessary to construct a multi-physical field neural network to invert the seepage parameters, i.e., to construct two neural networks, $\hat{H}(x;\theta_1)$ and $\hat{K}(x;\theta_2)$ to make the approximate estimation of the hydraulic head, $H(x)$ and $K(x)$, respectively, which is the same as that in the PINNs algorithm. At this time, θ_1 and θ_2 are the parameters to be optimized for the respective neural networks, and the total neural network parameters can be expressed as $\theta=\{\theta_1,\theta_2\}$. Accordingly, MSE_{PDE}, MSE_{BC} and MSE_{Data} become respectively:

$$MSE_{PDE}=\frac{1}{|\tau_P|}\sum_{x\in\tau_P}\left\|-\nabla^T(\hat{K}(x;\theta_2)\nabla\hat{H}(x;\theta_1))-W\right\|_2^2 \tag{22}$$

$$MSE_{BC}=\frac{1}{|\tau_B|}\sum_{x\in\tau_B}\left\|\mathrm{B}\left(\hat{H}(x;\theta_1)\right)\right\|_2^2 \tag{23}$$

$$MSE_{Data}=\frac{1}{|\tau_D|}\sum_{x\in\tau_D}\left\|\hat{H}(x;\theta_1)-H(x_D)\right\|_2^2 \tag{24}$$

The final parameter $\hat{\theta}$ can be obtained by optimizing the MSE with the optimization algorithm:

$$(\hat{\theta})=\arg\min_{\theta_1,\theta_2}MSE(\theta_1,\theta_2) \tag{25}$$

III. Specific manifestations of the impact of groundwater seepage on the stability of pit works

III. A. Impact of groundwater seepage on geotechnical bodies of pit works

The effects of groundwater seepage on the geotechnical body of foundation pit engineering mainly include physical, chemical and mechanical effects. Firstly, the physical effect of groundwater seepage on the geotechnical body refers to the water molecules forming a water film on the surface of the mineral under the control of the potential energy of the mineral surface, which in turn produces lubrication, softening and muddying, freezing and thawing on the geotechnical body; secondly, the chemical effect of groundwater seepage on the geotechnical body of the foundation pit project refers to the ionic exchange between the water and the geotechnical body, the oxidation reduction, the hydration, the dissolution and erosion and so on, which affects the geotechnical body's strength; finally, the mechanical influence mainly refers to the fact that the water in the rock body is not controlled by the

adsorption force on the surface of minerals, but by gravity, which produces latent corrosion, dissolution, and pressure effects on the geotechnical body.

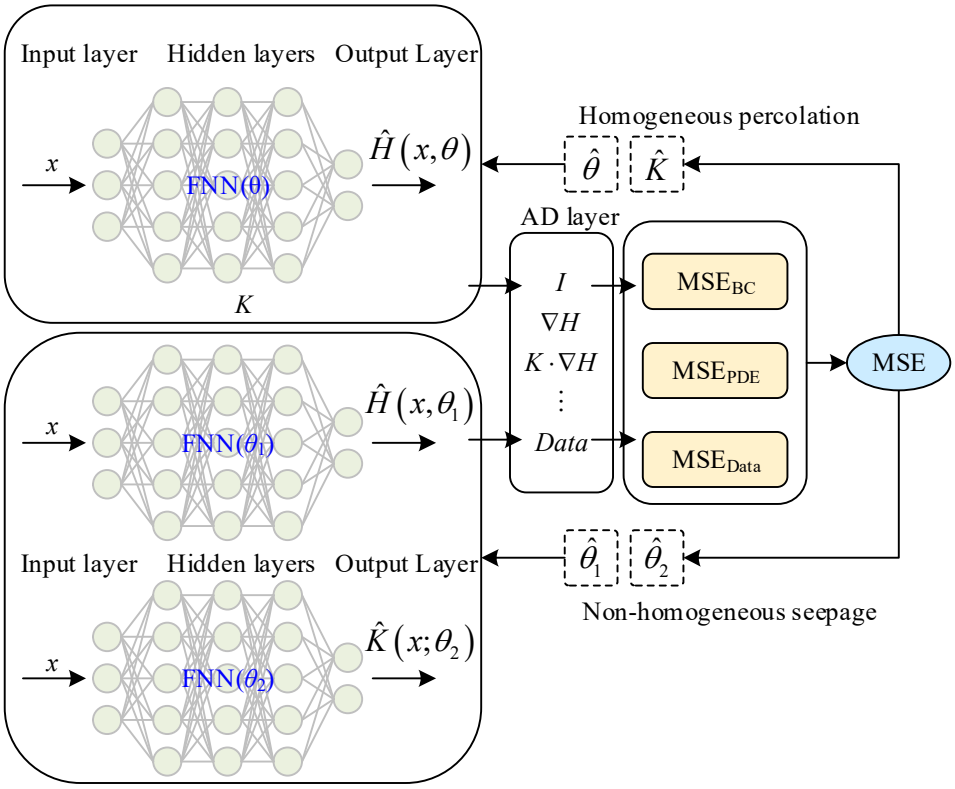

Figure 1: PINNs algorithms for identifying seepage parameters

III. B. Effects of groundwater seepage on foundation soil nails

In the soil nail support construction of foundation pit excavation, soil nails play an important role in the stability of the whole support structure. The anchoring effect of soil nails on the soil body of the foundation pit is mainly based on the frictional resistance and adhesive force generated by the contact between the interface of the soil body and the outer surface of the soil nails, while the seepage of groundwater will increase the water content of the soil body and reduce the frictional resistance between soil particles, which in turn affects the force between the soil nails of the foundation pit and the soil body. In the pit project, when the mortar and concrete solidification, the interior will produce many micro-cracks, these cracks will adsorb the underground seepage water, and form a water-rich zone around the pit soil body, under the adsorption of soil pore water, groundwater seepage will form a cohesive film of water, tightly wrapped around the surface of the soil nails, isolate the soil body from the soil nails, and reduce the degree of adhesion between the two.

In addition, under the action of hydrostatic pressure, the shear degree of the soil body will be reduced, coupled with the influence of groundwater infiltration, the pit slope soil body will produce internal micro-cracks, and cracks have a tendency to increase through, resulting in the pit soil body will occur small displacement, due to the water-rich areas of the parts of the impact of the different, coupled with the pit of the spatial effect of the pit, the pit in different parts of the soil nails wall will be subjected to uneven force, which in turn increase the load borne by the soil nails. At this time, if the tension force is greater than the anchoring force of soil nails, soil nails will be displaced, thus affecting the anchoring and skeleton in the soil body of the foundation pit, which shows that the soil nails of the foundation pit excavation and reinforcement of the significant role. However, in the actual construction process, due to the influence of groundwater seepage will cause great damage to the stability of soil nail support.

IV. Impact analysis of groundwater seepage in geotechnical engineering

In this paper, a large-scale cross-river highway bridge group project in southwest China is selected as the research object, the main span of the project adopts double-tower cable-stayed bridge structure, with the main girder

spanning up to 1200 meters, and the foundation of the bridge piers adopts group pile foundation system, with the maximum diameter of drilled piles of 3.5 meters and the depth of up to 95 meters. Engineering investigation reveals the existence of hidden karst collapse body in the bridge site area, the drilling process repeatedly exposed 1-3 meters in diameter of the cavern, the filler is dominated by a mixture of fluid-plastic powdery clay and gravelly debris, and locally see modern dissolution fissure seepage phenomenon.

The 3D modeling size is 70m×110m×65m, with displacement constraints in the X and Y directions around the model, displacement constraints in the Z direction at the bottom, and a free surface at the top. The soil body and diaphragm wall are modeled as solid units, and the beam unit model is selected for the internal support. The inner and outer surfaces of the diaphragm wall are used as the main surfaces in face-to-face contact, and the surfaces of the soil layer in contact with the wall are used as the slave surfaces. The soil body is modeled by Moore-Cullen principal model, and the numerical calculations are performed by numerical simulation software, which simulates the seepage force acting on the soil layer by setting different water level lines inside and outside of the foundation pit respectively, and solves the groundwater seepage model and inverts the parameters by using the PINNs algorithm.

IV. A. Algorithm validation

In order to illustrate the validity of the method proposed in this paper, we choose a two-dimensional unsteady flow in a nonhomogeneous isotropic pressurized aquifer as an ideal model for calculation. We first assume that the initial and boundary conditions of the model as well as the zoning parameters are known, so that the heads at several hypothetical observation points can be calculated by the finite element method, and then these heads are regarded as “observation heads”, and then the joint inversion method proposed in this paper is utilized for the parameter inversion, to check whether the results of the inversion parameters can be returned to the “true value” or not. The results of the inversion parameters are examined to see whether they can return to the “true value”.

Suppose that the confined aquifer area is a square with a length on one side, the east-west boundary is the fixed head boundary, the water head is H1, the north-south boundary is the waterproof boundary, and there is a pumping well in the center of the area to pump water with a flow rate Q, and the water conductivity of the confined aquifer is T. Let a=2000m, the boundaries AB and DC are the water barrier boundaries, AD and BC are the fixed head boundaries, and H1=150m. The number of triangular elements is 400 and the number of nodes is 195. The calculation is divided into three parameter partitions, a pumping hole is set at the point of P_1 in the center of the region, the pumping flow rate $Q=8000m^3/d$, the unit of the water conductivity T is m^2/d, the water storage coefficient S is a dimensionless variable, the unit of H is m, the elevation of the top and bottom plate of the aquifer is 65m and 0m respectively, the thickness of the aquifer M is 65m, and an observation hole OBS1, OBS2, OBS3 is set in the three parameter partitions respectively, The water level observations calculated using the finite element method are shown in Table 1. The hydrogeological parameters were inverted based on the water level observations.

Table 1: Observation data of water level in the observation hole

Time/d	OBS1 hole water level/m	OBS2 hole water level/m	OBS3 hole water level/m
0.500	99.3873	91.0378	99.0384
1.000	99.2284	90.9836	98.8937
1.500	99.1862	90.8362	98.8122
2.000	99.1754	90.7153	98.7256
2.500	99.0862	90.5621	98.6039
3.000	99.0274	90.4256	98.4935
3.500	98.9372	90.2852	98.4011
4.000	98.8251	90.0381	98.3274
4.500	98.6675	89.8376	98.2885
5.000	98.4183	89.7753	98.1937

The aforementioned PINNS algorithm is used for the inverse calculation, and the results are shown in Table 2. The objective function error shows a trend of rapid decline followed by oscillatory convergence with the increase in the number of iterations, and the error drops to 4.517E-02 at 100 generations, indicating that the algorithm already has a high efficiency in the initial parameter identification stage. The objective function error is only 1.974E-06 at 1000 generations.

Table 2: Inversion results

Algebra	Objective error function	$T_1/(m^2 \cdot d^{-1})$	$T_2/(m^2 \cdot d^{-1})$	$T_3/(m^2 \cdot d^{-1})$	S_1	S_2	S_3
5	4.028E+01	3018.2753353	198.4823537	1122.8656467	0.0285644	0.0129641	0.0738611
10	6.276E+00	301.4866478	147.9742474	894.8643561	0.0003825	0.0001756	0.0003754
20	5.286E-02	100.0186414	299.9997362	599.9999386	0.0001763	0.0004098	0.0005837
30	5.018E-02	100.0103862	299.9987631	599.9992751	0.0001786	0.0004083	0.0005888
50	4.836E-02	100.0099364	299.9977536	599.9982753	0.0001878	0.0004077	0.0005903
100	4.517E-02	100.0097365	299.9963641	599.9977351	0.0001901	0.0004046	0.0005911
200	4.216E-02	100.0089752	299.9951533	599.9963515	0.0001947	0.0004033	0.0005927
400	4.009E-02	100.0088375	299.9945134	599.9957531	0.0001983	0.0004019	0.0005973
600	3.762E-03	100.0086653	299.9938621	599.9948625	0.0001992	0.0004011	0.0005986
800	3.175E-04	100.0085038	299.9929863	599.9939275	0.0001997	0.0004007	0.0005991
1000	1.974E-06	100.0084200	299.9928300	599.9933100	0.0001999	0.0004002	0.0005999

The results of comparison of inversion parameters and truth values are shown in Table 3. By comparing the inversion parameters and true values in Table 3, the effectiveness of the PINNS algorithm in multi-parameter coupled inversion can be verified. The relative errors of hydraulic conductivity coefficients T_1-T_3 are less than 0.009%, which meet the requirements of engineering grade accuracy, and the absolute deviation of the inversion value of T_2 parameter, 299.99283m²/d, from the true value, 300m²/d, is only 0.00717m²/d, and the corresponding permeability coefficient error can be regarded as the equivalent and the same value in the engineering practice. The relative errors of the storage coefficients S_1-S_3 are controlled within 0.05%, and their numerical stability provides a reliable parameter basis for the pore water pressure field calculation.

Table 3: Comparison results of inversion parameters and truth values

Parameters	$T_1/(m^2 \cdot d^{-1})$	$T_2/(m^2 \cdot d^{-1})$	$T_3/(m^2 \cdot d^{-1})$	S_1	S_2	S_3
True value	100.0000000	300.0000000	600.0000000	0.0002000	0.0004000	0.0006000
Inversion value	100.0084200	299.9928300	599.9933100	0.0001999	0.0004002	0.0005999
Absolute error	0.0084200	0.0071700	0.0066900	1E-07	2E-07	1E-07
Relative error/%	0.0084200	0.0023900	0.0011150	0.0500000	0.0500000	0.0166667

IV. B. Impact of groundwater seepage on pit structures

IV. B. 1) Horizontal displacements of diaphragm walls

The horizontal displacements of diaphragm walls on the right side of different out-of-pit groundwater levels are shown in Figure 2. When the depth of diaphragm wall is less than 30m, the difference in horizontal displacement of diaphragm wall caused by different out-of-pit groundwater levels is more obvious, and when the depth is more than 30m, the difference in horizontal displacement of diaphragm wall caused by the four kinds of out-of-pit groundwater levels is not significant. This is due to the lack of support on one side of the diaphragm wall after pit excavation, resulting in large displacement under seepage, while the diaphragm wall located below the excavation depth will not produce large displacement due to the support of the soil on both sides. When the groundwater level outside the pit is -10m, the water level difference between inside and outside is large, under the joint action of water and soil pressure, the diaphragm wall produces a large horizontal displacement of 52.02mm, which reaches the maximum limit of horizontal displacement of diaphragm wall of 30mm~50mm as stipulated in the standard, and it is necessary to take measures to improve its safety. When the groundwater level outside the pit is -20m, -30m and -40m, the horizontal displacement of the wall does not change much, and the maximum displacement is located near the top of the pit, with the maximum horizontal displacement of 32.07mm, which is within the safety range.

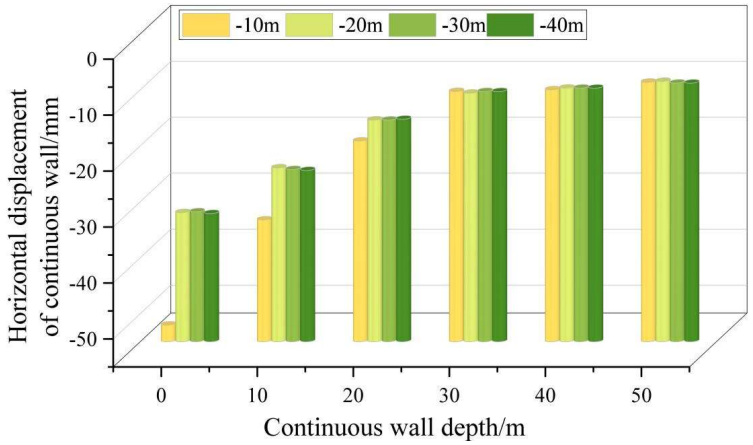

Figure 2: Foundation pit displacement at subsurface water levels outside different pits

IV. B. 2) Settlement of surrounding surface soils

Taking the right edge of the pit as the starting point and the horizontal distance of 30m from the edge of the pit as the end point, the amount of surface soil settlement within the range on the right side of the pit was studied. The surface soil settlement around the pit with different out-of-pit groundwater levels is shown in Figure 3. The trend of surface soil settlement under different out-of-pit water table conditions is basically the same, and the soil settlement curve is similar to a funnel shape, with the maximum surface settlement occurring at 10m from the pit, followed by a gradual decrease in soil settlement and a tendency to 0. Due to the overall length of the model is small and the assumption of a high water table, and also taking into consideration of the software's computational error, there is a slight soil augmentation at a distance of more than 20m from the edge of the pit and the soil settlement is slightly higher than that of the pit, and the settlement is slightly higher than that of the groundwater table when the distance is far enough away. When the distance is far enough, the settlement will tend to 0. When the groundwater level outside the pit is -10m, the maximum settlement is -18.39mm, which is less than the standard 25mm~3mm, and is within the safe range. When the groundwater level outside the pit is located at -20m, -30m and -40m, the surface settlement is small, at this time the maximum settlement is about -3.16mm, and the pit excavation construction is safer.

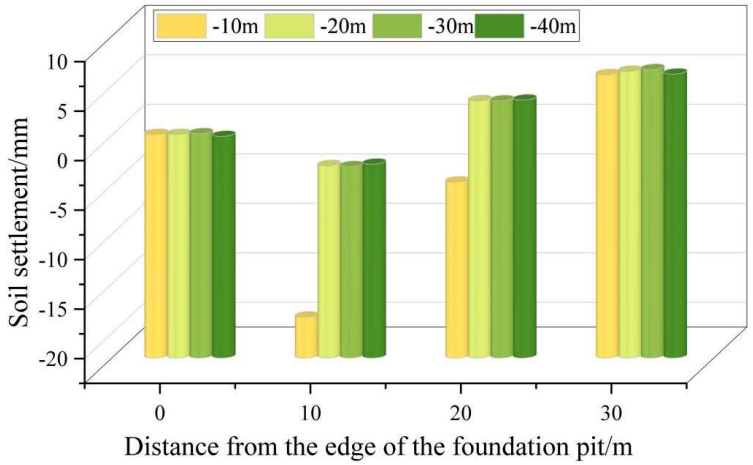

Figure 3: Horizontal displacement outside different pits

IV. C. Impact of groundwater seepage on project stability

Three monitoring points around the project were recorded in the numerical simulation. According to the calculation results, the change curves of settlement of the arch, horizontal convergence and arch base uplift with the discount factor are plotted for the two cases of groundwater seepage and indirect coupling of flow and solid, and groundwater seepage and complete coupling of flow and solid, and the discount factor corresponding to the sudden change in the curve of the displacement-decrease factor change is the safety coefficient of the project.

Groundwater seepage and fluid-solid indirect coupling engineering characteristic point displacement with the change curve of the discount factor is shown in Figure 4. The settlement and horizontal convergence of the arch top are much larger than the deformation of the arch bottom bulge, and the growth of the arch bottom bulge with the strength reduction factor is not obvious. When the strength discount factor is greater than 5.78, the settlement of the arch top and the horizontal displacement of the arch girdle increase sharply, and the calculated engineering safety factor is 5.78.

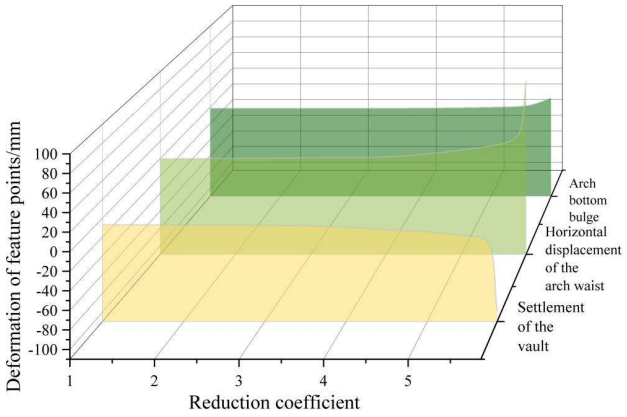

Figure 4: Fluid-structure indirect coupling

The change curves of the displacement of engineering characteristic point with the discount factor when groundwater seepage and fluid-solid coupling is complete are shown in Fig. 5. The settlement of the arch top and horizontal displacement of the arch waist increase sharply when the strength reduction factor is more than 5.52, and the engineering safety factor is 5.52 under this condition.

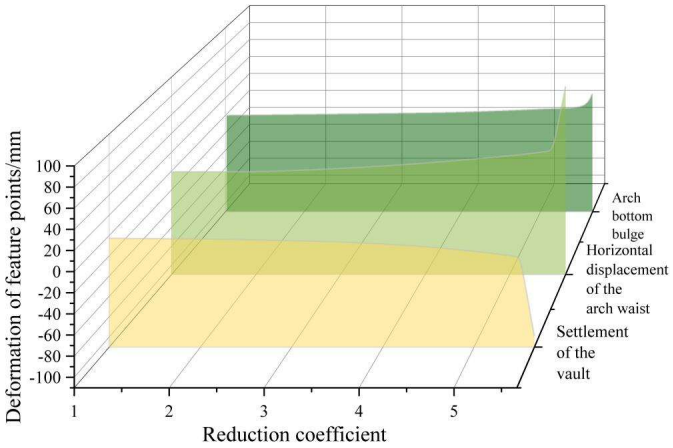

Figure 5: Fluid-structure complete coupling

Comparing the calculation results of the two cases, it can be found that the calculation results of groundwater seepage and full fluid-solid coupling are slightly smaller than that of groundwater seepage and indirect fluid-solid coupling, which is due to the use of the indirect fluid-solid coupling mode, which weakened the interaction between seepage field and stress field.

V. Conclusion

This paper discusses the influence of groundwater seepage on the stability of foundation engineering in geotechnical engineering, and solves the groundwater seepage model and parameter inversion based on PINNs algorithm.

In the ideal model, the relative errors of the PINNs algorithm for solving the hydraulic conductivity coefficients T_1-T_3 are all less than 0.009%, which meet the requirements of engineering level accuracy, among which the absolute deviation of the inversion value of T_2 parameter 299.99283m²/d from the true value of 300m²/d is only 0.00717m²/d, and the corresponding permeability coefficient error is considered to be the equivalent and the same value in the

engineering practice. The relative error of water storage coefficient S_1-S_3 is controlled within 0.05%, and its numerical stability provides a reliable parameter basis for pore water pressure field calculation.

In the research model, when the depth of diaphragm wall is less than 30m, the difference in horizontal displacement of diaphragm wall caused by different out-of-pit groundwater levels is more obvious, and when the depth is more than 30m, the difference in horizontal displacement of diaphragm wall caused by four kinds of out-of-pit groundwater levels is not significant. When the groundwater level outside the pit is -10m, the difference between the internal and external water levels is large, and under the joint action of water and soil pressure, the diaphragm wall produces a large horizontal displacement, which reaches 52.02mm. When the groundwater level outside the pit is -20m, -30m and -40m, the horizontal displacement of the wall does not change much, and the maximum displacement is located near the top of the pit, with a maximum horizontal displacement of 32.07mm, which is within the safe range. Under different conditions of groundwater level outside the pit, the trend of surface soil settlement is basically the same, the soil settlement curve is similar to funnel shape, the maximum surface settlement occurs at 10m from the pit, and then the soil settlement gradually decreases and tends to 0. When the groundwater level outside the pit is -10m, the maximum settlement is -18.39mm, which is less than the standard of 25mm~3mm, and it is in the safe range. When the groundwater level outside the pit is located in -20m, -30m and -40m, the surface settlement is small, at this time the maximum settlement is about -3.16mm, the pit excavation construction is safer.

The maximum settlement is about -3.16mm, which is safer for foundation excavation. When groundwater seepage and indirect coupling of flow and solid, the settlement of arch top and horizontal convergence are much larger than the deformation of arch bottom bulge, and the growth of arch bottom bulge is not obvious with the strength reduction coefficient, and the engineering safety coefficient is 5.78. When groundwater seepage and complete coupling of flow and solid, the settlement of arch top and the horizontal displacement of arch waist increase dramatically with strength reduction coefficient larger than 5.52, and the engineering safety coefficient is 5.52.

Funding

This work was supported by Natural Science Foundation of Henan Province, China (242300420316).

References

[1] Maca, N., Dietz, K., Stille, H., & Virely, D. (2023). Rock engineering design in tomorrow's geotechnical toolbox: Eurocode 7–Geotechnical structures: Anchors, rock bolts soil nails, and groundwater control (EN 1997-3: 2024). Geomechanics and Tunnelling, 16(5), 536-558.

[2] Mather, J. (2020). Relationship between rock, soil and groundwater compositions. In Geochemical Processes, Weathering and Groundwater Recharge in Catchments (pp. 305-328). CRC Press.

[3] Zhang, W., Wang, W., Zhou, D., Zhang, R., Goh, A. T. C., & Hou, Z. (2018). Influence of groundwater drawdown on excavation responses–A case history in Bukit Timah granitic residual soils. Journal of Rock Mechanics and Geotechnical Engineering, 10(5), 856-864.

[4] Preene, M., & Chrimes, M. M. (2021). Groundwater lowering for construction of the Kilsby Tunnel, UK–geological and geotechnical aspects. Proceedings of the Institution of Civil Engineers-Engineering History and Heritage, 175(4), 130-144.

[5] Hu, J., & Li, X. (2024). Deformation mechanism and treatment effect of deeply excavated expansive soil slopes with high groundwater level: Case study of MR-SNWTP, China. Transportation Geotechnics, 46, 101253.

[6] He, X., Shi, W., Zhu, Y., Yan, L., Zhao, Y., & Wang, S. (2025). Coupled Effects of Fault-Related Groundwater Flow and Pore Water Pressure: Unraveling the Mechanisms of Deformation and Failure in Gentle Slopes. Arabian Journal for Science and Engineering, 1-18.

[7] Yao, Y., Zhang, M., Deng, Y., Dong, Y., Wu, X., & Kuang, X. (2021). Evaluation of environmental engineering geology issues caused by rising groundwater levels in Xi'an, China. Engineering Geology, 294, 106350.

[8] Zhang, S., Xu, Q., Peng, D., Zhu, Z., Li, W., Wong, H., & Shen, P. (2020). Stability analysis of rock wedge slide subjected to groundwater dynamic evolution. Engineering geology, 270, 105528.

[9] Ge, X., Gao, Y., Jiang, Y., Zhao, X., Wu, K., Zhang, J., ... & Wang, Q. (2023). Influence of groundwater level change on deep foundation pit and its control technology. In E3S Web of Conferences (Vol. 394, p. 01006). EDP Sciences.

[10] Wang, Z., Bi, L., Kwon, S., Qiao, L., & Li, W. (2020). The effects of hydro-mechanical coupling in fractured rock mass on groundwater inflow into underground openings. Tunnelling and Underground Space Technology, 103, 103489.

[11] Zhang, W., Zhang, L., Gao, Y., Gao, X., Zhang, H., & Yu, M. (2019). The annual fluctuation of underground temperature response caused by ground heat exchanger in the condition of groundwater seepage. Energy and Buildings, 186, 37-45.

[12] Zhou, C. B., Chen, Y. F., Hu, R., & Yang, Z. (2023). Groundwater flow through fractured rocks and seepage control in geotechnical engineering: Theories and practices. Journal of Rock Mechanics and Geotechnical Engineering, 15(1), 1-36.

[13] Bao, J., Wang, K., Han, K., Xie, Y., & Luo, J. (2025). Influence process and mechanism of high-to low-permeability zones on the groundwater seepage field and solute transport in alluvial fans. Journal of Environmental Chemical Engineering, 13(2), 115982.

[14] Liu, G., Zheng, F., Jia, L., Jia, Y., Zhang, X. C. J., Hu, F., & Zhang, J. (2019). Interactive effects of raindrop impact and groundwater seepage on soil erosion. Journal of Hydrology, 578, 124066.

[15] Abdullah, T. O., Ali, S. S., Al-Ansari, N. A., Knutsson, S., & Laue, J. (2020). Magnitude and Direction of Groundwater Seepage Velocity in Different Soil and Rock Materials. Engineering, 12(4), 242-253.